

INFLUENCE OF SURFACE TREATMENT AND DESIGN OF 3D-REINFORCEMENTS ON DELAMINATION RESISTANCE & MECHANICAL PROPERTIES OF CFRP/CFRP JOINTS UNDER STATIC & FATIGUE LOADING

M. Juergens^{1,3}, A. Kurtovic¹, T. Mertens¹, M. Kolb¹, D. Greitemeier¹, H. Lang², E. Hombergsmeier¹, K. Drechsler³

¹Airbus Group Innovations
P.O. Box 800465, D-81663 Munich, Germany
Email: michael.m.juergens@airbus.com, web page: <http://www.airbusgroup.com>

²Fraunhofer ICT
Am Technologiezentrum 2, D-86159 Augsburg, Germany
Email: holger.lang@ict.fraunhofer.de, web page: <http://www.ict.fraunhofer.de>

³Institute for Carbon Composites, Technische Universität München
Boltzmannstraße 15, D-85748 Garching, Germany
Email: drechsler@lcc.mw.tum.de, web page: <http://www.lcc.mw.tum.de>

Keywords: Delamination resistance, Z-reinforcements, Structural joints/joining

ABSTRACT

Structural joint design strongly determines the weight saving potential of carbon fiber reinforced polymers (CFRP) in primary aircraft structures. The introduction of through-thickness reinforcements into the joining area addresses the issue of an efficient load transfer between laminates and adherents to increase delamination resistance and thus improve damage tolerance. In the present work, an innovative process is presented for a cost and time-efficient manufacture, with multidimensional metallic structures enhancing the joint's interlaminar fracture toughness. Spikes bent in the out-of-plane direction made of stainless steel and titanium were exposed to wet-chemical (HF/HNO₃, Turco 5578®) and physical (pulsed laser irradiation; Nd:YVO₄, 1064 nm) surface treatments to create micro- and nano-scaled oxide layer morphologies respectively.

A single lap shear (SLS) geometry was chosen to determine an optimized spike density and layout under static and fatigue load for the aimed application of the stringer run-out area in the lower aircraft fuselage. mode II strain energy release rate (SERR) was then determined and proved to increase considerably through the introduction of pretreated reinforcements into an end notched flexure (ENF) joint geometry. Laser irradiation on titanium reinforcements shows a superior performance when compared to alkaline etched or baseline sandblasted spikes. Surface analytics through scanning electron microscopy (SEM) and x-ray photoelectron spectroscopy (XPS) was employed to further correlate fracture mechanical results to the oxide surface chemistry, morphology and contamination, resulting from the applied co-bonding process.

1 INTRODUCTION

Carbon-fiber reinforced polymer (CFRP) laminates feature weight saving benefits gained by superior specific in-plane strength and load-related dimensioning, which leads to their increasing use in primary aircraft structures [1]. Considering the anisotropic material behavior and laminar structure of CFRP, major challenges arise in the field of structural joint design. Their load carrying fiber structure and out-of-plane properties have to be considered [2]. Adhesive bonding of composite joints respects the fiber structure and integrates curing of both CFRP and adhesive into one process; yet shortcomings such as poor out-of-plane properties, difficult joint failure prediction and a lack of

appropriate non-destructive testing (NDT) methods demand a more damage tolerant joining technology. So-called "chicken rivets" are currently used as the state-of-the-art technology in aerospace primary structures to generate a secondary load path which however interrupts the load carrying fiber structure of the composite. The fibers are cut when drilling the laminate, its cross-section is reduced significantly and delamination may occur in the surrounding area [3].

Various z-reinforcement technologies have been developed with the goal of mechanically interlocking adhesively bonded CFRP adherents. Progress has been made on methods like Z-pinning [4,5], HYPER joints [6] and CMT welded pins [7] to name a few.

An innovative joining technique features a low-thickness sheet of stainless steel or titanium with out-of-plane bent reinforcing elements, positioned between two CFRP adherents before or during the co-bonding process [8,9,10]. These out-of-plane directed spikes were proven to work as damage arresting features to the joint by creating a secondary load path through a meso-scale mechanical interlocking. This work is dedicated to a further improvement of the delamination resistance of a co-bonded CFRP joint applying this technology. Related research revealed considerably raised strain energy release rates (SERR) under mode I and mode II loading for z-pinned laminates [12-19]. Unlike single carbon fiber (CF) pins, the continuous metallic structure of the sheet bending technique allows to benefit from the increased surface by pretreating it and in this way enable further mechanical interlocking with the surrounding epoxy resin / adhesive in a range from micro- to even nanoscaled morphologies. Contrary to elastic dominated fracture mechanical properties of CF z-pins, plastic shear deformation of metallic reinforcements is expected to add an additional energy absorbing mechanism.

The quality of such adhesively bonded hybrid joints is critically affected by the applied surface pretreatment [20]. With the co-bonding process considered in this work, before both curing, i.e. the bonding cycle, the respective polymer adherent is in an uncured state. Hence, the metal reinforcement surface is the only one to be pretreated. Various techniques were developed for an enhanced long-term durable adhesion on titanium and stainless steel [20,21,32,33]. Wet-chemical processes like alkaline etching and anodizing were observed to be successful in nano-structuring the surface and in this way significantly improving bonding behaviour. Environmental issues and unique bath setups for different metals and alloys as major drawbacks are incentivating alternative physical techniques to be developed [22,32]. Titanium ($\alpha + \beta$ - alloy) surfaces were successfully modified on a nano-range by laser irradiation, improving joint strength due to an increased surface area in [22-27]. Chemical activation, contamination removal and the impact of the angle of incidence on the resulting surface morphology were studied in [28].

Previous work proofed the discussed technology's potential to almost double the delamination resistance of metallic z-reinforced CFRP joints under mode I loading [11]. In this paper, z-reinforcements for co-bonded ENF specimens are demonstrated to increase mode II interlaminar fracture toughness values by 75 %. Laser irradiation of titanium sheets further increases the strain energy release rate (SERR) significantly compared to the sandblasted baseline. By means of chemical characterization (XPS), wet-chemically treated sheets were revealed to still show co-bonding process-related contaminations and thus, do not contribute to the fracture mechanical CF/epoxy joint properties. A single lap shear (SLS) fatigue testing campaign was performed in order to derive an approximation of an optimal pin-density concerning the focused final application of a stringer run-out area. Complementary tests under static loading conditions were presented in [9].

2 MANUFACTURING

Earlier publications were dedicated to the development and improvement of the applied approach of integrating the reinforcing metal sheets into a co-bonded joint of prepreg laminates [8,9,11]. Consecutive stamping and bending of endless sheets was performed in an integrated tooling developed by Hölzel Stanz- und Feinwerktechnik GmbH+Co. KG. Five SLS and four ENF specimens of each configuration were manufactured with the same curing cycle, in a two-step process. The specimen's structure is depicted in Figure 1:

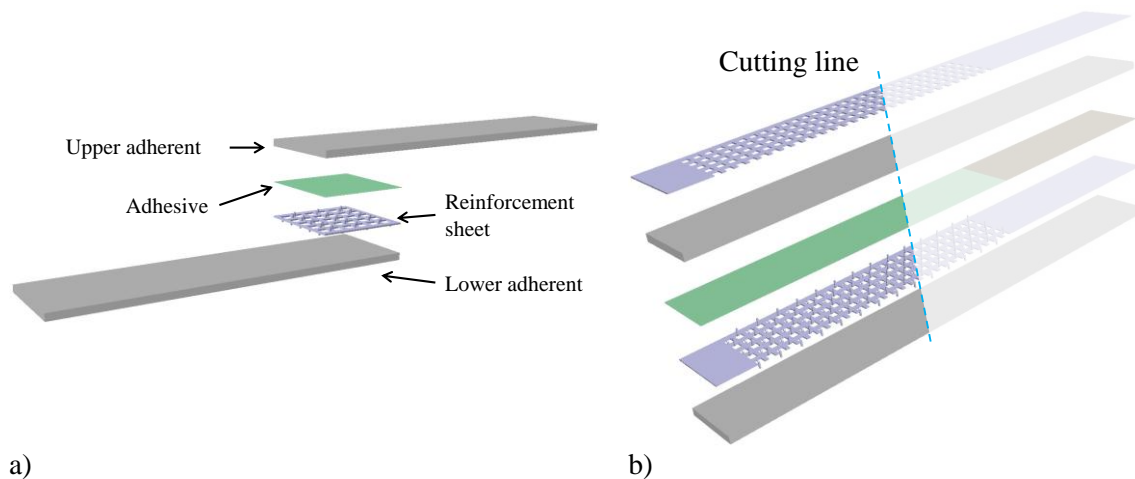


Figure 1: a) SLS and b) ENF specimen structure (ENF specimens cut from respective double cantilever beam (DCB) counterparts, tested in [11])

The reinforcement sheets featuring the above mentioned varying spike densities (SLS) and pretreatments (ENF) penetrates the lower CFRP adherent during the first autoclave cycle by simply realigning the carbon fibers. To ensure a rubber residue-free surface and to prevent the spike's bending while maintaining an even pressure level on the layup, a flexible, silicone containing plate is applied on the sheet. For the ENF specimens, a Teflon foil is placed above the film adhesive on the cured part to create an artificial precrack on the specimen; these are then followed by the uncured upper adherent. To compensate the bending stiffness, ENF specimens feature another metal sheet. The same metal as the reinforcement sheet is applied, featuring identical dimensions but without out-of-plane bent spikes.

3 EXPERIMENTATION

3.1 Materials

Specimen adherents were manufactured from HexPly® M21/198/T800S medium grade unidirectional prepreg, provided by the Hexcel Corporation. A quasi-isotropic layup $\{0/90/0/-45/+45\}_S$ was used to compose ENF laminates with a nominal thickness of 1.93 mm. SLS adherents' stacking sequence was mirrored $\{+45/-45/0/90/0\}_S$ in accordance to previous work [9]. FM® 300M epoxy film adhesive supplied by Cytec Industries was applied for the bonding of all specimens discussed in this work. For all ENF specimens investigated, an overall layup following $\{[0/90/0/-45/+45]_S\}/\text{metal}[[[0/90/0/-45/+45]_S]/\text{metal}$ resulted, “[|” indicating the precrack position induced by a prior mode I testing procedure (see

Figure 1). For the overlap area of the reinforced SLS joints, a layup following $\{[+45/-45/0/90/0]_S\}/\text{metal}[[[+45/-45/0/90/0]_S]$ was applied respectively.

For matters of cost-efficiency, reinforcement sheets for the SLS specimens were manufactured from stainless steel SAE 304 only and both, stainless steel and titanium was applied for the determination of mode II fracture toughness. The meta-stable β -alloy Ti 15-3 (AMS 4914A, aerospace specification) by Timet Inc. was used to produce reinforcement sheets of 0.4 mm thickness each, since commonly used $\alpha+\beta$ -alloys lack of cold formability. With regard to the comparatively large joining area, ENF specimen bending caused by deviating coefficients of thermal expansion (CTE) of CFRP and metal was present only to a barely visible extent, compared to the stainless steel (SAE 304 / 1.4301) reinforced joints.

For SLS reinforcement sheets, areal pin densities of 0.6 %, 0.7 %, 1.2 % and 1.4 % were chosen, similar to configurations tested in previous work under static loading. A density of 1.2 % was determined under static [9] and fatigue loading to allow an optimal pin-spacing to address the trade-off between the weakening of the metal/CFRP-interface and the increasing of the interlocking between the spikes and the laminates. Results derived under fatigue loading are presented and discussed in detail in paragraphs 4 and 5. This pin spacing was consecutively applied for the ENF testing campaign.

3.2 Surface pretreatment

Al₂O₃ (grain size: 250-500 μm, blasting pressure: 7 bar) was used for the *mechanical surface pretreatment* to roughen and increase the active surface. A consecutive plasma irradiation was chosen to chemically convert process-related contaminations (e.g. silicone residues) into compounds that are less harmless to adhesion properties.

Prior to the *wet-chemical surface pretreatment*, all sheet surfaces were cleaned with an alkaline solution of P3 Almeco 18, 30 g/l (Henkel) at 60 °C ± 3 for 15 min. Etched titanium and stainless steel sheets were exposed to Turco 5578@ 500 g/l (Henkel) and a 40/52 % HF/HNO₃ solution respectively. The alkaline process was set up under 95 °C for 5 min, whereas acid etching was performed at RT for 5 min.

Laser surface pretreatment was performed similar to the procedure presented in [22]. A Powerline E25 system (Rofin-Sinar Laser, Nd:YVO4) was used to generate short pulsed laser irradiation (wavelength: 1064 nm). A set of parameters for laser induced nano-structuring was developed by Kurtovic [22] for Ti-6Al-4V which was applied for the physical pretreatment of both, beta-alloy Ti 15-3 and SAE 304 stainless steel. The carrying sheet was focused horizontally in a 90 deg angle to the normal incidence in ambient atmosphere. Since the reinforcing spikes are bent in z-direction, the sheet was inclined so that a maximum contingence angle of 60 deg was realized, limited by geometrical constraints [11].

3.4 X-ray photoelectron spectroscopy (XPS) / scanning electron microscopy (SEM)

A Quantum 20000 spectrophotometer (Physical Electronics) was used to post surface treatment analyse selected surfaces. A monochromatic source AlKα (1486.6 eV) featuring base pressures less than 10⁻⁶ Pa under a take-off angle of 45 deg was used to obtain the spectra at a spot size of 200 μm. The survey spectra (117.4 eV pass energy) were quantified calculating spectras' peak area after background subtraction by integration and multiplying by sensitivity factors according to Moulder [29]. Survey spectra evaluation was performed software-aided (Multipak V. 9.3); results were normalized to 100 at%.

Morphology characterization in a top and a side view (cryo fracture) analysis was performed using a Zeiss Aurisa field emission SEM. The specimens were sputter coated with Platinum to avoid charging.

3.5 Fatigue life, lap shear

SLS fatigue testing was conducted at RT, employing a frequency of 10 Hz and a stress ratio of R = 0.1. Max. stresses were chosen between 0.5 σ_{max} and 0.65 σ_{max} of a co-bonded joint's static shear strength. Crack propagation was recorded at four spots to estimate the crack fronts' position at the upper and lower overlap edges respectively.

3.5 Interlaminar fracture toughness, mode II: G_{IIc}

All specimens were tested at a constant cross-head speed of 1 mm/min. Results were analysed using the beam theory. A correction factor Δ_{II} was added to the measured crack length to take account of the adherents' bending beyond the crack tip during testing:

$$G_{IIc} = \frac{9F(a + |\Delta_{II}|)^2\delta}{2b(2L^3 + 3(a + |\Delta_{II}|)^3)} \quad (1)$$

Required dimensions (*b* – specimen width, *L* – half span length) were measured prior to testing. The crosshead displacement *δ*, resulting force *F* and crack length *a* were recorded during the testing procedure. G_{IIc} values for all configurations were calculated based upon the crack length *a* at the initial force drop under displacement controlled loading. In addition, forces for fixed values of crack propagation were recorded to create R-curves also pre and post force drop.

4 RESULTS

4.1 Reinforcement sheet surface morphology and contamination

As indicated in [10], morphologies of Ti 15-3 and SAE 304 after laser irradiation (Figure 2, 60 deg angle of incidence) show a homogenous open porous nano structure similar to the investigations of Kurtovic [22,23]; dimensions below 100 nm were created on the titanium β -alloy as well as on the steel substrate. Thicknesses of $161 \text{ nm} \pm 15$ (titanium) and $109 \text{ nm} \pm 9$ (steel) were measured for the oxide layers created the surfaces respectively. The limitation of the angle of incidence on the spikes to 60 deg is due to the low-distance, subsequent spike positioning on the sheet [10].

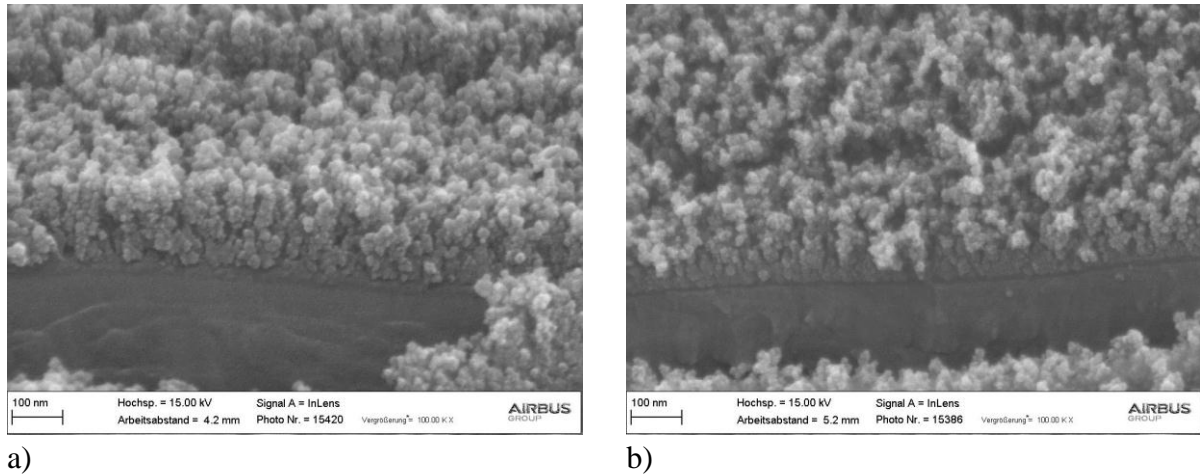


Figure 2: SEM micrographs depicting high magnification detail of a) Ti 15-3 and b) St 1.4301 surface morphology after laser pretreatment (cryo fracture side view, 60 deg angle of incidence) [10]

Two more major differences in surface morphologies were revealed by the SEM micrographs (Figure 2). Both, cross-sectional and top shape of the ridges and cavities are more coarse and rough for the titanium substrate. However, in the nano-scale a smoother transition zone towards the bulk material is visible. In addition, right below the nano-structure, the steel substrates show a thin gap at the interface to the bulk material.

Micrographs for wet-chemical and grit blast treated sheets shown in [10] reveal group 3 and group 1 topographies [24] respectively (group 1: no micro- / no macro-roughness, group 2: macro-roughness, group 3: micro-roughness). No nano-scaled but a smooth (SAE 304) and a slightly (Ti 15-3) structured morphology was created by alkaline or acid etching, as documented in previous work [22,30,35]. Titanium samples showed a fragmented, brittle fracture-like surface after grit blasting due to its lower ductility compared to the austenitic steel. For both materials, Al_2O_3 residues were visible.

Selected steel surfaces were pre- and post-pretreatment analyzed by XPS with respect to the fracture mechanical testing data (Figure 4) was conducted by XPS and results are shown in Table 1.

Table 1: pre- and post-pretreatment surface analysis (SAE 304) [10]

Condition	C / at%	O / at%	Si / at%	Si2p / eV
Initial state after 1 st curing cycle	58,9	24,4	16,5	102,32 (silicone)
Plasma treated after 1 st curing cycle	23,5	55,7	15,6	103,39 (silicate)
Laser treated after 1 st curing cycle	28,1	54,5	0	-/-

Carbon and silicon compounds indicate the degree of contamination. Both physical means of

pretreatments, plasma (initially wet chemically treated) and laser irradiation (initially laser treated) after the first curing cycle significantly reduce carbon residues on the respective surfaces. On the plasma treated surfaces, silicon compounds were proven in the form of silicate; no silicon residues at all could be detected for the laser treated surfaces within the information depth of 3-5 nm.

4.2 Fatigue life, lap shear

Crack propagation behavior and the impact of reinforcement spacing and array on fatigue life (SLS geometry) is depicted in Figure 3. The spike density is defined and varied by the *sheet thickness* (0.2 mm vs. 0.4 mm), *slope array* (6 longitudinal rows of 5 vs. 6 spikes in specimen width) and *amount of spikes per window* (1 vs. 2) chosen.

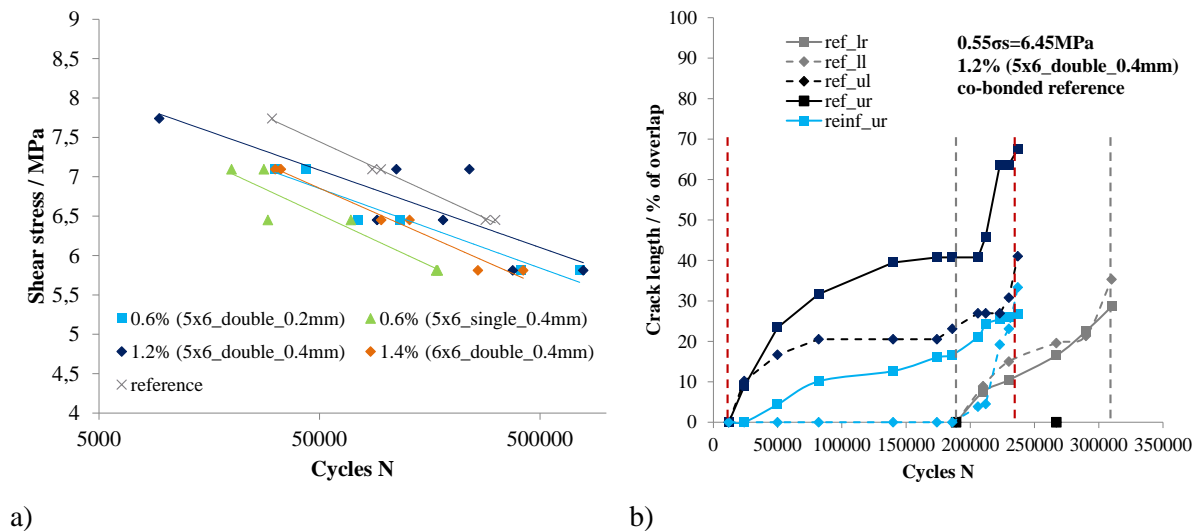


Figure 3: a) fatigue life in dependency of spike density and b) crack propagation behavior of reinforced SLS joints

All configurations tested, including the co-bonded reference, show a similar sensitivity of fatigue life to the maximum stress applied. A density of 1.2 % resulted in an increase of the considered part of the woehler curve compared to a smaller (1.4 %) and higher (0.6 %) pin spacing. The reduction of sheet thickness results in a decrease of fatigue life, not to the same extent as the reduction of pin spacing though. Compared to the co-bonded reference, it needs to be stated that there was no significant increase in fatigue performance observed.

Figure 3 b) highlights the crack initiation and propagation behavior by the representative example of a reinforcement sheet featuring 0.4 mm thickness, 5 times 6 spikes and 2 spikes per window. The dashed lines indicate crack propagation period, red and grey colors representing the reinforced specimen and the co-bonded reference respectively. A clear shift of the crack initiation event is visible to a lower number of cycles for the reinforced joints. Yet, the crack propagation period is extended significantly compared to the co-bonded reference. Crack fronts are propagating asymmetrically in the reinforced joints with no overlap edge determined to be the preferred spot of crack initiation. A similar behavior was documented for the co-bonded reference, crack length to failure is reduced significantly though.

4.3 Interlaminar fracture toughness, mode II

Critical interlaminar fracture toughness (G_{IIc}) and underlying force vs. displacement plots are depicted in Figure 4. Delamination resistance based on the initial force drop during the displacement controlled testing procedure is increased in the range of + 31 % (wet-chemically treated titanium) to + 76 % (laser treated titanium) compared to the co-bonded baseline. Sand blasting was determined to be the most efficient treatment for the steel surfaces, almost reaching up to values of beams featuring

laser pretreated titanium ($3503 \text{ J/m}^2 \pm 183$ vs. $3516 \text{ J/m}^2 \pm 278$). The introduction of wet-chemically treated SAE 304 sheets led to the worst performance ($705 \text{ J/m}^2 \pm 144$) among all configurations tested.

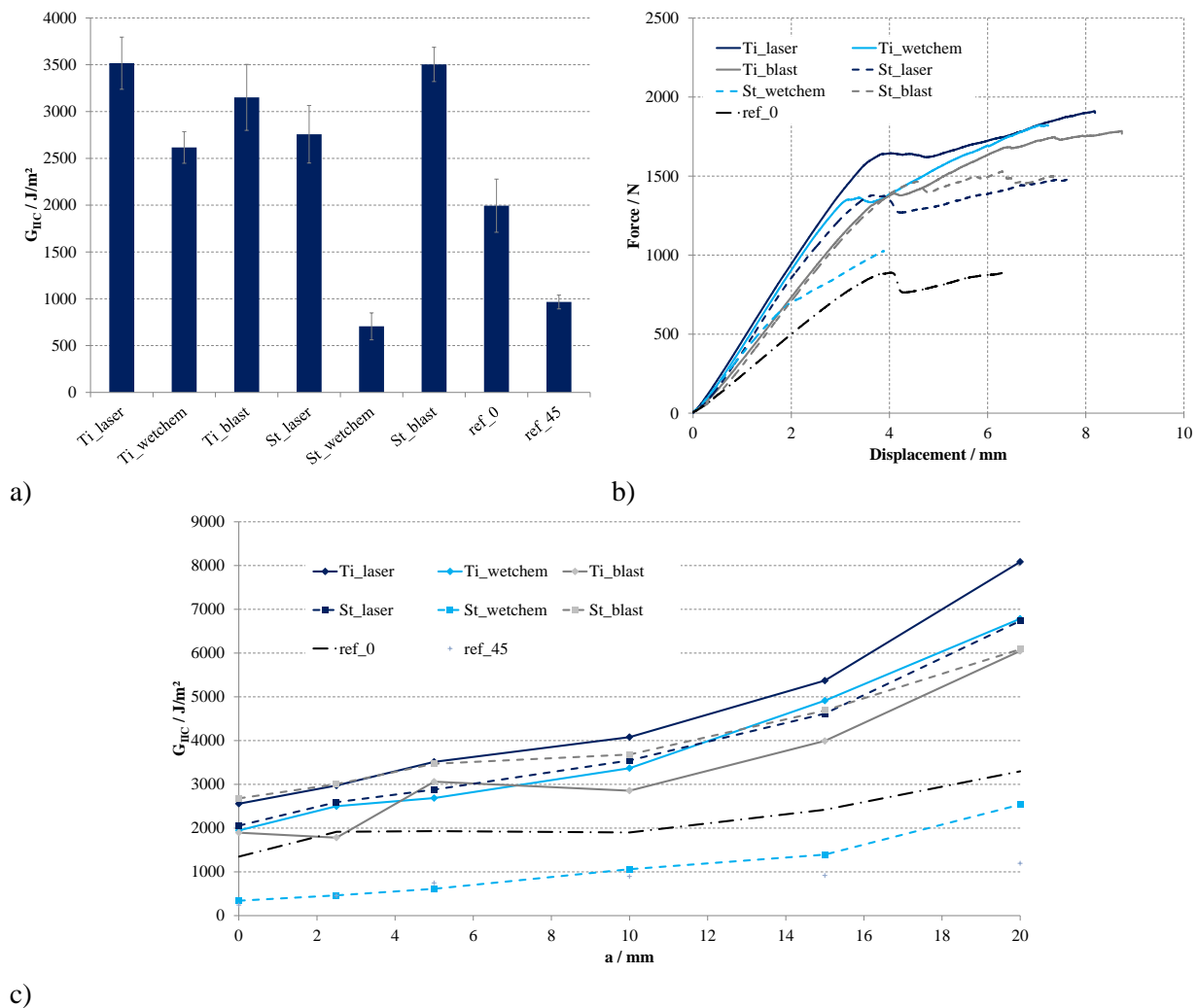


Figure 4: a) critical fracture toughness (G_{IIC}), b) force vs. displacement plot and c) r-curve for physically, wet-chemically and mechanically pretreated Ti 15-3 and SAE 304 reinforcement sheets

For all reinforced joints, compliance ranges between $2,31 \text{ m/N} \pm 0,2$ (Ti 15-3) and $2,55 \text{ m/N} \pm 0,2$ (SAE 304), which means a significant shift compared to the co-bonded baseline ($3,97 \text{ m/N} \pm 0,16$) due to the stiffening metal sheets between adherents and on top of the joint. Furthermore both reinforcing metals provoke an increase in F_{max} and $\delta_{max}(\Delta a = 20 \text{ mm})$ as depicted in in Figure 4 b), in particular pronounced for titanium reinforcements.

Considering the whole area below the $F(\delta)$ plot and the respective R-curves in in Figure 4 c) illustrates the increasing divergence of delamination resistance as a function of crack growth between reinforced joints and the co-bonded reference in general and the superior performance of laser pretreated Ti 15-3 reinforcements in particular. The r-curve progression post initial force drop is noticeable e.g. for beams featuring sandblasted SAE 304 sheets and Turco® treated sheets. A gain of energy needed for an increment of crack growth was calculated approx. only 75 % vs. 130 % respectively. Laser pretreatment of Ti 15-3 reinforcements results a similar shape/increase (133 %) with regard to a wet-chemical treatment. However both, actual values and relative increase post initial force drop are outperforming the co-bonded baseline whose $G_{IIC}(\Delta a = 20 \text{ mm}) = 3298 \text{ J/m}^2 \pm 326$ (gain of 72 %) is approached by joints featuring wet-chemically treated SAE 304 sheets ($2536 \text{ J/m}^2 \pm 750$; gain of 239 %) which did not show any adhesion at all (see 4.1).

5 DISCUSSION

The introduction of z-reinforcements into laminates or joints of laminates inevitably creates voids like fiber undulations and resin nests [9]. This detrimental effect of defects at overlap edges overcompensates the beneficial contribution of spikes to peel resistance. Once a crack is initiated by one of these bad spots, the amount of acting reinforcements is relatively low and increases the further the crack propagates. Hence, it is shown the major advantage of through-thickness reinforcements being the increased resistance to crack propagation post initiation which prevents joints from spontaneous failure as documented for the co-bonded reference SLS joints. This matches insights of related work on z-reinforced joints' mode I fracture toughness properties [11,14,15], stating delamination resistance to be lower in the early stage of crack propagation compared to simply bonded specimens. Obviously the stresses in the overlap area of a SLS geometry are increasing the further the crack propagates, explaining the above depicted poor performance with regard to outstanding results of mode I/II fracture toughness.

Mechanical interlocking on at least two scales was proven to significantly increase fracture toughness under mode II loading. Reinforcing metal spikes shift the level of energy needed for an incremental crack growth right from the start of the R-curves recorded. The further the crack grows, the more spikes are acting (debonding, snubbing, frictional pull-out [4]) and thus to be plastically deformed, unlike CF z-pins which experience elastic deformation only [16,17]. Contrary to mode I loading conditions, spikes are exposed to resulting stresses during the whole testing procedure unless they are sheared off, which was not the case in the present work. Moreover, crack closure forces are raised as the crack grows and shear/bending stress ratio spikes are exposed to, is increasing; in a disproportional manner with regard to frictional effects also occurring between co-bonded adherents (Figure 5).

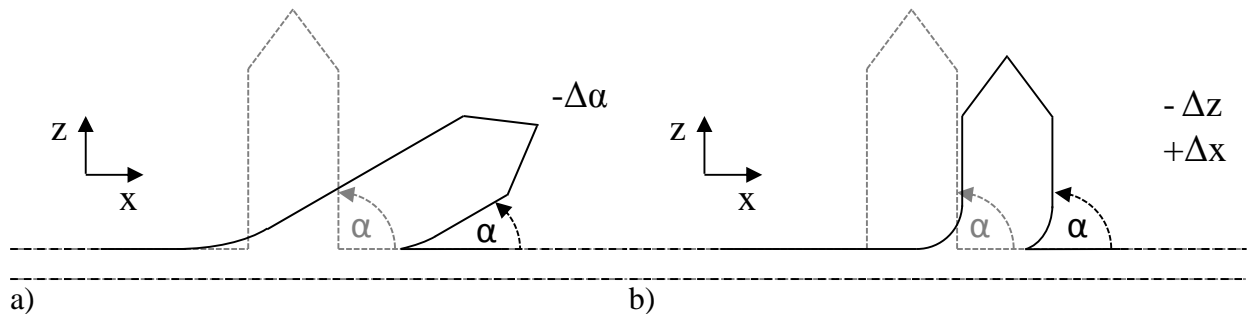


Figure 5: plastic deformation of metallic spikes a) bending dominated at $\Delta a = 0$ mm and b) shear dominated at $\Delta a = 20$ mm

This explains the strong increase of delamination resistance post initial force drop, particularly made visible by joints featuring wet-chemically treated SAE 304 sheets that did not show any adhesion at all. Secondly, as testing results and analytical techniques highlight, laser irradiation is capable of adding another level of interlocking on a nano-scale between metal substrate and epoxy, in this way further increasing and also activating the surface area with an increased number of covalent links on it [11,22,23,31]. Both, macroscopic z-reinforcements and a nano-scaled morphology on them create a multidimensional structuring that results in an increasing gap of delamination resistance between the laser pretreated Ti 15-3 and the co-bonded reference of up to $\Delta_{\max} G_{IIIC}(a = 20 \text{ mm}) = 4785 \text{ J/m}^2$. Fracture mechanical testing results of wet-chemically pretreated SAE 304 reinforcements indicate the latter named effect (nano-structuring) supporting the energy absorbing mechanism of plastic spike deformation (macro-structuring). The original shape of the R-curve representing interlocking on a macro-scale only is kept and, as a function of crack growth, increasingly shifted to higher G_{IIIC} values. This is most pronounced for laser pretreated Ti 15-3, but to a lower extent also valid for the remaining treatment/material combinations.

6 CONCLUSIONS

Delamination resistance of co-bonded CFRP joints is improved significantly introducing cost- and time-efficiently manufactured multidimensional metallic through-thickness reinforcements. Crack closing forces under mode II loading conditions causes the degree of metallic spikes' plastic deformation, i.e. energy absorption to increase disproportionately. A further dimension of mechanical interlocking on a nano-scale by laser irradiation is added to metallic, particularly titanium reinforcing sheets. In this way adhesion properties between the metal and the surrounding adhesive/resin epoxy is improved through an increased nano-structured, cleaned and chemically activated surface area. Hence, SERR of locally propagating crack fronts (e.g. between spikes and laminates; adhesion properties) contribute to the joint's global fracture toughness (plastic deformation of spikes, joint properties).

Future research will be dedicated to the determination of mode II fracture toughness after exposure to varying environmental conditions. Also, the energy absorbing mechanisms on a single-pin level will be determined and applied to analytically describe a joint's failure behaviour under mode I and mode II loading conditions. It is furthermore suggested to review the SLS joint design at the overlap edges to reduce the effect of defect introduced by z-reinforcements and increase their contribution to crack initiation and propagation.

ACKNOWLEDGEMENTS

We want to express our appreciation to the Federal Ministry of Education and Research, Germany, (BMBF) for funding this research within the TransHybrid project.

REFERENCES

- [1] M. C. Y. Niu, *Composite Airframe Structures*, Connilit Press, Hong Kong, 1996.
- [2] B. Kolesnikov, L. Herbeck, A. Fink, CFRP/titanium hybrid material for improving composite bolted joints, *Composite Structures*, **83**, 2008, pp. 368-380.
- [3] L. J. Hart-Smith, *Design and Analysis of bolted and riveted joints*, Ed. L. Tong. Recent advances in structural joints and repairs for composite materials, Kluwer Academic Publishers, Dordrecht, NL, 2003.
- [4] A. P. Mouritz, Review of z-pinned composite laminates, *Composites*, **38**, 2007, pp. 2383-2397.
- [5] I. K. Partridge, D. D. R. Cartié, T. Bonnington, *Manufacture and performance of z-pinned composites*, Eds. G. Shonaike, S. Advani. Advanced polymeric composites. CRC Press, Boca Raton (FL), US, 2003.
- [6] P. N. Parkes, R. Butler, D. P. Almond, Growth of damage in additively manufactured metal-composite joints, *15th European Conference on Composite Materials, Venice, IT*, 2012.
- [7] S. Stelzer, S. Ucsnik, J. Tauchner, T. Unger, G. Pinter, Novel composite-composite joining technology with through thickness reinforcement for enhanced damage tolerance, *The 19th International Conference on Composite Materials, Montreal, CA*, 2013.
- [8] A. C. Nogueira, K. Drechsler, E. Hombergsmeier, Analysis of the Static and Fatigue Strength of a Damage Tolerant 3D-reinforced Joining Technology on Composite Single Lap Joints, *53rd AIAA/ASME/ASCE/AHS/ASC Structures, Structural Dynamics and Materials Conference. Honolulu (HI), US*, 2012.
- [9] M. Juergens, A. C. Nogueira, H. Lang, E. Hombergsmeier, K. Drechsler, Influence of an optimized 3d-reinforcement layout on the structural mechanics of co-bonded cfrp joints, *16th European Conference on Composite Materials, Seville, ES*, 2014.
- [10] H. Lang, A. C. Nogueira, M. Juergens, E. Hombergsmeier, K. Drechsler, Numerical Investigation on the structural Mechanics of a Joining Technique for Composite Materials: The redundant high Efficiency Assembly, *16th European Conference on Composite Materials, Seville, ES*, 2014.

- [11] M. Juergens, A. Kurtovic, T. Mertens, A. C. Nogueira, H. Lang, M. Kolb, P. Strobach, E. Hombergsmeier, K. Drechsler, Effect of surface treatment for metallic z-reinforcements on interlaminar fracture toughness of cfrp/cfrp joints, *Proceedings of 29th International SAMPE Tech. Conf. 2015, Baltimore (MD), US, May 18-21, 2015*, Society for the Advancement of Material and Process Engineering, 2015.
- [12] D. D. R. Cartié, *Effect of Z-Fibres™ on the Delamination Behaviour of Carbon Fibre / Epoxy Laminates*, Doctoral thesis, Cranfield University Library, Cranfield (UK), 2000.
- [13] D. D. R. Cartié, J. M. Laffaille, I. K. Partridge, A. J. Brunner, Fatigue delamination behaviour of unidirectional carbon fibre/epoxy laminates reinforced by Z-Fiber® pinning, *Engineering Fracture Mechanics*, **76**, 2009, pp. 2834-2845.
- [14] L. G. Stringer, M. J. Hiley, Through-thickness reinforcement of composites: z-pinning, stitching and 3-D weaving., *14th International Conference on Composite Materials, San Diego (CA), US, 2003*.
- [15] M. Troulis, D. D. R. Cartié, L. Bartattoni, I. K. Partridge, Z-Pinned woven laminates: Interlaminar fracture results and pinning quality considerations, *6th International Conference on Deformation and Fracture of Composites, Manchester, UK, 2001*.
- [16] D. D. R. Cartié, B. N. Cox, B. N. Fleck, Mechanisms of crack bridging by composite and metallic rods, *Composites*, **35A**, 2004, pp. 1325-1336.
- [17] K. L. Rugg, B. N. Cox, R. Massabò, Mixed mode delamination of polymer composite laminates reinforced through the thickness by z-fibres, *Composites*, **33**, 2002, pp. 177-190.
- [18] M. Hojo, K. Nakashima, T. Kusaka, M. Tanaka, T. Adachi, T. Fukuoka, M. Ishibashi, Mode I fatigue delamination of Zanchor-reinforced CF/epoxy laminates, *International Journal of Fatigue*, **32**, 2010, pp. 37-45.
- [19] K. Pingkarawat, A. P. Mouritz, Improving the mode I delamination fatigue resistance of composites using z-pins, *Composites Science and Technology*, **92**, 2014, pp. 70-76.
- [20] A. Baldan, Review: adhesively bonded joints and repairs in metallic alloy, polymers and composite materials: adhesives, adhesion theories and surface pretreatment, *Journal of Materials Science*, **39**, 2004, pp. 1-49.
- [21] T. Mertens, H. Kollek, On the stability and composition of oxide layers on pre-treated titanium, *International Journal of Adhesion and Adhesives*, **30**, 2010, pp. 466-477.
- [22] A. Kurtovic, E. Brandl, T. Mertens, H. J. Maier, Laser induced surface nano-structuring of Ti-6Al-4V for adhesive bonding, *International Journal of Adhesion and Adhesives*, **45**, 2013, pp. 112-117.
- [23] A. Kurtovic, T. Mertens, M. Kolb, H. J. Maier, Surface structuring of Ti-6Al-4V for adhesive bonding by laser irradiation: formation of nanostructures, *Proceedings of the 29th International SAMPE Tech. Conf. 2014, Seattle (WA), US, June 2-5, 2014*, Society for the Advancement of Material and Process Engineering.
- [24] J. D. Venable, Review: Adhesion and durability of metal-polymer bonds, *Journal of Materials Science*, **19**, 1984, pp. 2431-2453.
- [25] E. G. Baburaj, D. Starikov, J. Evans, Enhancement of adhesive joint strength by laser surface modification, *International Journal of Adhesion and Adhesives*, **27**, 2007, pp. 268-276.
- [26] P. Molitor, T. Young, Investigations into the use of excimer laser irradiation as a titanium alloy surface treatment in a metal to composite adhesive bond, *International Journal of Adhesion and Adhesives*, **24**, 2007, pp. 127-134.
- [27] A. Y. Vorobyev, G. Chunlei, Femtosecond laser structuring of titanium implants, *Applied Surface Science*, **253**, 2007, pp. 7272-7280.
- [28] R. Rechner, I. Jansen, E. Beyer, Influence on the strength and aging resistance of aluminium joints by laser pre-treatment and surface modification, *International Journal of Adhesion and Adhesives*, **30**, 2010, pp. 595-601.

- [29] J. F. Moulder, J. Chastain, W. F. Stickle, P. E. Sobol, K. D. Bomben, *Handbook of x-ray photoelectron spectroscopy: a reference book of standard spectra for identification and interpretation of XPS data*, Physical Electronics, Chanhassen (MN), US, 1995.
- [30] T. Mertens, F. J. Gammel, M. Kolb, O. Rohr, L. Kotte, S. Tschöcke, S. Kaskel, U. Krupp, Investigation of surface pre-treatments for the structural bonding of titanium, *International Journal of Adhesion and Adhesives*, **34**, 2012, pp. 46-54.
- [31] A. Kurtovic, *Laserinduzierte Nanostrukturierung von Titanoberflächen für das strukturelle Kleben – Einfluss auf die Oberflächenmorphologie, Ermüdungs- und Adhäsionseigenschaften*, Doctoral Thesis. Universitätsbibliothek Paderborn, Paderborn, DE, 2014.
- [32] R. Broad, J. French, J. Sauer, CLP new, effective, ecological surface pretreatment for highly durable adhesively bonded metal joints, *International Journal of Adhesion and Adhesives*, **19**, 1999, pp. 193-198.
- [33] T. S. Williams, D. Cheng, R. F. Hicks, Atmospheric pressure plasma as a method for improving the adhesive bonding properties of metals and composites, *Proceedings of the 29th International SAMPE Tech. Conf. 2014, Seattle (WA), US, June 2-5, 2014*, Society for the Advancement of Material and Process Engineering.
- [34] F. Bouquet, J. M. Cuntz, C. Coddet, Influence of surface treatment on the durability of stainless steel sheets bonded with epoxy, *Journal of Adhesion Science and Technology*, **6**, 1992, pp. 233-242.
- [35] B. S. Covino, J. V. Scalera, T. J. Driscoll, J. P. Carter, Dissolution behavior of 304 stainless steel in HNO₃/HF mixtures, *Metallurgical Transactions A*, **17**, 1986, pp. 137-149.